ORCAS - Keck Instrument Development - ORKID

Eliad Peretz[a], Peter Wizinowich[b], Bert Pasquale[a], Guillaume Filion[d], Maxwell A. Miller-Blanchaer[c], John Mather[a], Shui Hung Kwok[b], Scott Lilley[b], Jean Thomas Landry[d], Luke Gers[b], Eduardo Marin[b], Sam Ragland[b], Ed Wetherell[b], Jason Chin[b], Rebecca Jensen-Clem[e], Peter Kurczynski[a], Shobita Satyapal[f], Peter Plavchan[f], Étienne Gauvin[d], Imke de Pater[g], Steph Sallum[h], and Eric Nielsen[i]

[a]NASA Goddard Space Flight Center, Greenbelt, MD 20771, USA
[b]W. M. Keck Observatory, Mauna Kea, HI 96781, USA
[c]University of California Santa Barbara, CA 91125, USA
[d]OMP inc., Quebec City, Qc, G1K 4L2, Canada
[e]University of California, Santa Cruz, Santa Cruz, CA 95064, USA
[f]George Mason University, Fairfax, Virginia 22030, USA
[g]University of California, Berkeley, Berkeley, CA, USA
[h]University of California Irvine, Irvine, CA 92697, USA
[i]New Mexico State University, Las Cruces, NM 88003, USA

ABSTRACT

A new breed of space-ground hybrid observatory, the Orbiting Configurable Artificial Star (ORCAS) mission is working with the W. M. Keck Observatory (WMKO) to demonstrate the viability of diffraction-limited visible imaging from large ground telescopes. To support that, we have built and delivered ORKID (The ORCAS Keck Instrument Demonstrator) as an early visible-wavelength performance demonstration with the Keck II Adaptive Optics (AO) system. By enabling AO and flux calibration observations, the low-cost ORCAS/ORKID mission will deliver highly detailed images to support many scientific advances. A community driven observation plan will provide Great Observatory quality capabilities open to all US observers. These observations will result in unique science for the mission, while also complementing and extending space-borne science.

Keywords: ORCAS, W. M. Keck Observatory, Adaptive Optics, Artificial Guide Star, Orbiting Guide Star, Wavefront Correction, Visible Instrument, Hybrid Observatories

1. INTRODUCTION

The Orbiting Configurable Artificial Star (ORCAS) mission is a first-of-its-kind hybrid space and ground observatory. It aims to enable new science otherwise only accessible to future flagship-class missions over a decade from now, at a SmallSat budget, by providing unprecedented angular resolution, exquisite sensitivity and a unique flux calibrator to ground observatories. By enabling adaptive optics (AO) and flux calibration observations, ORCAS will deliver highly detailed images, unlocking the ability to detect a population of supermassive black hole binaries for the first time, among many other advances. The low-cost ORCAS mission operating in collaboration with the W. M. Keck Observatory (WMKO) will provide Great Observatory quality capabilities open to all US observers via a community driven observation plan. These observations will result in unique science for the mission, while also complementing and extending the science of HST, JWST and Roman, as well as other potential future missions.

The ORCAS mission (include citations of past ORCAS papers (about 7)) would provide a source for AO wavefront sensing allowing correction at visible wavelengths with the WMKO AO systems (Wizinowich2000,2006). To support that, we have built and delivered ORKID (ORCAS Keck Instrument Demonstrator) as an early visible-wavelength performance demonstration with the Keck II AO system. ORKID uses a fast camera that

Further author information: E-mail: eliad.peretz@nasa.gov

will initially allow it to be used for lucky imaging. A planned upgrade of the Keck II AO system to a higher order system will facilitate direct (non-lucky) imaging when using bright guide stars. ORKID will also provide the Keck II AO system with the capability to do future visible science demonstrations, anywhere in the sky, with ORCAS.

In this paper we establish the scientific and programmatic goals in section 2, formulate the instrument engineering requirements section 3, share details of the optical and mechanical design of the instrument in section 4, conduct performance analysis in section 5, and finally share initial on-sky performance of the system in section **??**.

2. SCIENTIFIC AND PROGRAMMATIC GOALS

2.1 Science

ORKID has been designed to open the doors to a range of new exciting scientific studies in a range of astronomical fields. Here we highlight the primary science cases for ORKID, broken up into four main groups: Solar System, Binary Stars, Accreting Exoplanets and Active Galactic Nuclei.

2.1.1 Solar System Science

In the decades since the Voyager spacecraft flew past Neptune and Uranus,[1,2] the two planets have changed significantly. Uranus, initially devoid of significant cloud features has revealed several large cloud features since the planet's north pole came into view.[3] Neptune, on the other-hand, has demonstrated a continuous evolution, with dark spots and bright clouds frequently appearing and disappearing$^{e.g.}$.[4] Understanding the atmospheric dynamics that cause these features is a key step in understanding the detailed atmospheric structure of these planets and progress can only be made through multi-wavelength (and hence multi-pressure-level) monitoring.

Ground-based observations in visible wavelengths would bring a wealth of additional information to ground-based NIR observations since different atmospheric depths are probed at different wavelengths. ORKID will enable monitoring of the two planets the two planets in and out of the methane band at wavelengths, 889 and 643 nm, respectively. The contrast between clouds and background is highest at 889 nm, where we probe near the tropopause, while deeper layers are probed at 643 nm. This data can be compared with NIR images, and extend wavelength (i.e. altitude) coverage of previous Keck data.

Titan's atmosphere consists primarily of N_2 gas with a few percent CH_4. Since Titan's surface temperature is close to the triple point of CH_4, this compound behaves like water on Earth. A dense haze layer, produced via photolysis of CH_4 prevents probing the surface, except at a few wavelengths in the IR and at 940 nm. ORKID will observe both at 889 and 940 nm to probe both the atmosphere and surface, respectively. We expect these atmospheric and surface maps to produce the highest resolution features since Cassini, allowing us to search for changes in time.

2.1.2 Binary Stars

With the high spatial resolution afforded by ORKID, new stellar binaries can be imaged and the orbits of known binaries can be monitored with higher astrometric precision as compared to the infrared. This could benefit a range of binary star science cases, including the dynamic measurement of stellar masses. While there are many situations where this might be useful, here we describe one such case: the estimation of the ages of young moving groups.

To determine robust masses for imaged substellar companions it is essential to have a well-defined age for the system. The host stars of most imaged planets to date reside in nearby young moving groups. A common method to determine the age of a young moving group it to use the HR diagram position of the stars in the group combined with models of stellar evolution to find a best-fit age for all the stars in the group. Measuring dynamical masses of moving group binary stars presents an opportunity to improve on this method, as they eliminate the degeneracy between mass, metallicity, and age in the color-magnitude diagram. By combining resolved photometry and a dynamical mass measurements one can use a consistent framework to determine the age probability distribution of each component, and so directly measure the age of the entire moving group.

Observations of binary stars with ORKID are not only expected to provide improved astrometric precision over NIR measurements because of the smaller PSF (improving the dynamical mass estimates), but the new wavelength range will provide a critical lever arm on the stellar atmospheric models. To provide the best constraints on the stellar models ORKID will require R, I and z band measurements. To obtain the highest spatial resolution ORKID requires fast-read modes for Lucky/Speckle Imaging at the shortest wavelengths and a non-redundant masking mode to push to the smallest angular separations.

2.1.3 Accreting Exoplanets

Despite the thousands of known planets, the early stages of planet formation are poorly constrained by observations. In particular, the details of mass delivery mechanisms and timescales at early ages are difficult to probe due to the paucity of accretion measurements. So far accretion has been directly detected in only three cases: the controversial LkCa 15b,[5–7] PDS 70 b and c,[8,9] and Delorme 1 (AB)b,[10] despite several searches.[11,12] These initial detections have allowed us to start constraining models Choksi2022, but more measurements are needed. Leveraging Keck's near-infrared Pyramid wavefront sensor[13] and its large aperture, the short wavelength coverage afforded by ORKID will enable new searches for H-alpha emission from accreting protoplanets around redder stars and at smaller inner working angles than previously accessible. These searches require the ORKID filter complement to include an H-alpha narrow-band filter, and a continuum filter. When searching for accreting planets, ORKID will operate in a lucky imaging mode, a speckle imaging mode and/or a non-redundant masking mode.

2.1.4 Active Galactic Nuclei

Astro2020 articulated the importance of understanding the role of SMBHs in galaxy evolution. The vast majority of galaxies are believed to host SMBHs, and they are known to regulate star formation; they are a key source of energy in the galaxy ecosystem

Dual AGN are expected because galaxies grow and evolve via mergers and interactions, yet observations of dual AGN are exceedingly rare. Observing them is important because they provide evidence of black hole growth through accretion, regulation of star formation, and they are precursors of black hole mergers, which are strong emitters of gravitational radiation.

Final parsec problem: it is especially important to probe close in mergers because of the difficulty with which theoretical models account for how SMBHs go from close encounters to candidates for merger. To date there is only one bound binary known[14] and only a handful with separations less than 3 kpc.[15–18] Current Keck AO can only resolve dual AGN to $\sim$ 50 pc resolution. At this distance, SMBH are not yet gravitationally bound. However, diffraction limited optical observations can probe this close-in region.

Resolve nuclear star clusters near the AGN

Nuclear star clusters are typically 3 pc in size. We would get unprecedented spatial information for the firs time. Color gradients would constrain star formation history and growth. This can be done with greater resolution than HST. We can estimate masses (I band observations have been used for this; see ref X). Ideal targets may be non-active galaxies or type 2 AGN, where contamination of the continuum by the AGN is less significant.

Discuss specific targets, goals of optical observations of AGN (?)

Discuss outflows and star formation in AGN (?). We are sensitive to Hα, which is a recent SFR indicator. Can Hα be used to measure SFR density in the inner region close to the AGN, or are there other confounding sources of Hα from the AGN itself (?)

2.2 Programmatic Goals

A major goal this effort is to demonstrate and characterize the performance of the current Keck II AO system at visible wavelengths. By doing so both retiring risk, raising technology readiness level (TRL), and informing the future design of ORCAS-WMKO mission instruments.

We are interested in using the Pyramid and Shack-Hartmann wavefront sensors for:

1. Measuring the Strehl ratio and FWHM in short (10 ms) and long exposures (several minutes) over a range of wavelengths (0.6 to 0.9 um) and guide star magnitudes (0 to 10th).

2. The contrast ratio versus distance from the guide star.

3. Better understand the limitations of the current Keck AO system and what performance improvements are needed for impactful ORCAS science.

4. How much tip-tilt performance improvement is needed to maintain close to diffraction-limited angular resolution. (This can be seen in the evolution of image position between consecutive short exposure images).

5. Use this experience as a step in developing a roadmap to visible science instrumentation to be developed for ORCAS.

6. Longer term the camera should be usable to take short exposure images of a spacecraft as it transits the science field.

Write about: Commissioning an instrument in high-speed, building a team between NASA and Keck.

3. INSTRUMENT REQUIREMENTS, CONSTRAINTS AND DESIGN CHOICES

The ORKID design is driven by the scientific and programmatic requirements presented in section 2.

The physical location and size for a visible science camera was limited by the constraints of the Keck II AO bench. ORKID needed to be located in reflection from the dichroic beamsplitter that transmits light to the near-infrared science instruments. It could not interfere with the light that goes to the existing visible wavefront sensors. A decision was therefore made to integrate a visible science camera with the existing acquisition camera (ACAM) as part of the ORKID package.

A second decision that drove the design was the selection of an Andor Marana-4BV11 camera for the ORKID science camera. The Marana camera met the ORKID speed requirements and is already used as a guider camera at Keck, including as the ACAM camera.

3.1 Science Camera Opto-Mechanical Requirements

The following requirements were established for the science camera:

1. The visible science camera system shall be Nyquist sampled at 650 nm wavelength. Discussion: Nyquist sampling at 650 nm requires 6.7 mas/pixel.

2. The plate scale shall be met within a tolerance of $\pm$ 0.1 mas.

3. The visible science camera system shall provide a 10" or larger unvignetted science field.

4. The transmitted wavefront quality through the visible camera system optics shall be less than 50 nm rms. Discussion: 50 nm is a Strehl reduction of 0.67 at 500 nm.

5. The throughput through the visible camera system optics shall be greater than 90 percent between 500 and 950 nm wavelength.

6. A 2"x2" science field shall be capable of being read out in 10 ms.

7. Differential atmospheric refraction (DAR) correction must be provided between the science and wavefront sensing wavelengths to maintain the science target position within 1/4-wavelength over a 5 minute observation sequence at 45° zenith angle.

8. Differential atmospheric refraction over any 100 nm wavelength band between 600 and 1000 nm shall be less than 1/4-wavelength at 45° zenith angle.

9. The visible science camera system shall provide a filter changer with at least six filter locations.

10. The filter changer shall be located as close as possible to the pupil plane to minimize field dependent aberrations and to allow a pupil plane mask to be located in the filter wheel. 11. The visible science camera system shall be provided with the a science determined set of filters.

12. The visible camera system shall not vignette the 120" diameter field to the AO acquisition camera.

13. The visible camera system shall be co-mounted on the same stage with the AO acquisition camera.

14. A beamsplitter shall be provided to split the 500 to 950 nm light between the visible science camera and the AO acquisition camera.

3.2 Footprint, Volume and Weight Constraints

The ORKID assembly and its location on the AO bench are shown in Figure 1. The horizontal footprint of the existing ACAM system could not be exceeded to avoid interference with existing opto-mechanics. The vertical height was limited by the position of the optical axis above the AO bench (305mm) and the height of the AO bench cover. The clearance of the delivered ORKID unit (vertical space between the unit and the AO bench cover) is 54mm. ACAM is mounted on a linear stage and pedestal which were reused to support ORKID. The stage is used to focus ACAM on either a natural guide star (at infinity) or a laser guide star (as close as 85km). If necessary, the handles shown in Figure 1(a) can be removed to reduce the footprint.

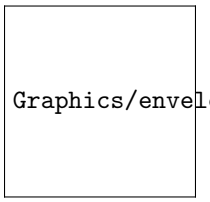

Figure 1. Envelope available to integrate the ORKID unit on the AO bench of Keck II.

An astigmatism corrector plate, mounted to the front of the ORKID assembly, extends outside the current ACAM envelope. This assembly fits in the AO bench CAD model but the actual space on the bench will be validated prior to installation (the corrector can be removed if necessary).

The maximum weight for the ORKID unit was set by the maximum allowed weight for the linear stage (90kg). However, due to the difficult installation access to the AO bench, the unit was designed to minimize weight.

4. INSTRUMENT DESIGN

4.1 Optical Design

The ORKID optical system includes the acquisition channel (previously ACAM) and the science channel. (See Fig. 2) The driving performance goal was 2-pixel sampling of a 650 nm diffraction-limited PSF FWHM to meet the Rayleigh criteria. The main design constraint was the volumetric limits for being able to be placed on the very crowded Keck AO bench.

4.1.1 Optical Layout

The ORKID instrument features a 100mm acceptance aperture, which is placed at the focus of the AO bench visible light path. At a plate scale of 0.727 mm/arc second, this allows for the capture of the 120 arc second diameter circular field passed through the AO rotator. A 250 mm focal length field lens converges the ray bundles to form a pupil at the acquisition camera lens. The 50 mm f/1.4 lens re-images the incoming telescope image onto the acquisition camera sensor

Within the converging ray bundle following the field lens, a dichroic beamsplitter reflects the long wavelengths (greater than 615 nm) to the science channel. A custom triplet lens captures the central 10 arc second field to re-image it at the science camera at f/??? (??? Meter focal length). At a camera plate scale of 6.7”/pixel, the 650 nm point spread function FWHM falls within two pixels.

Before reaching focus, the beam passes through several more optical elements. A pair of filter wheels, each with six positions, allow for bandpass filters and/or pupil masks to be placed into the beam. The first filter wheel is located at the pupil formed by the combination of the field lens and the triplet. It is there that either four filters or a pupil mask can be inserted into the beam. The pupil mask is used for Non-redundant Aperture Masking Interferometry (AMI) for increased angular resolution of a specific binary target. The second filter wheel contains five additional bandpass filters. Either filter wheel can be used in the ”open position”, and the

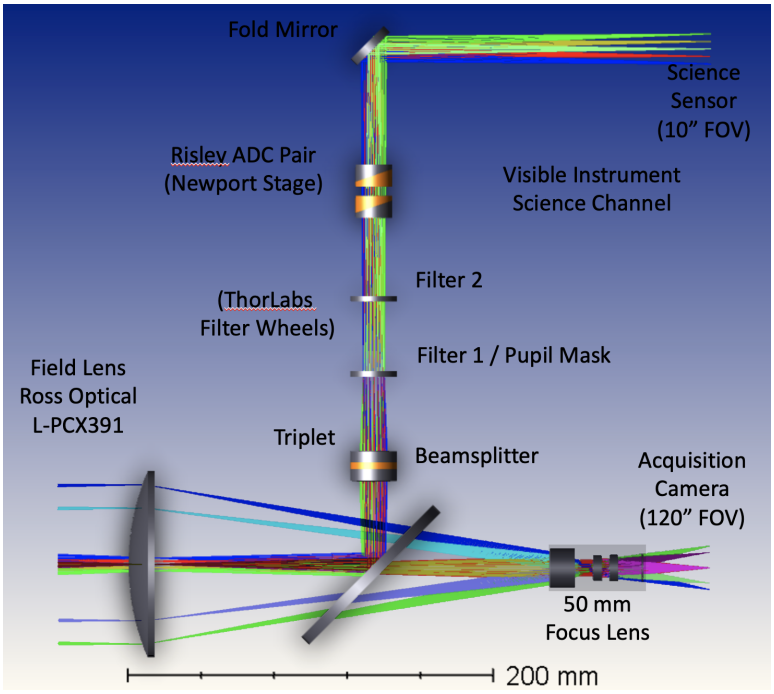

Figure 2. Optical Layout of the ORKID instrument.

filters in the second wheel can be used in conjunction with the pupil mask of the first wheel. The second filter wheel is tilted by 2° to avoid additional ghost reflections between the two filter wheels.

The next element in the optical train is the atmospheric dispersion correction (ADC) consisting of a Risley doublet prism pair mounted in dual rotation stages. At Keck's magnification, when looking at an object 60° off zenith, the resulting spectrum from 600 to 950 nm is about 1.5 mm long due to atmospheric dispersion. The ADC prisms consist of a cemented pair of high dispersion / low dispersion (but matched index) glasses which can act in concert to correct the atmospheric dispersion. When counter rotated 90°, they cancel each other out and have no dispersive effect. The ADC prisms rotate counter-rotate to provide the correct amount of dispersive correction and co-rotate to maintain the zenith direction. Note that for narrow band filters, dispersive correction is not needed, but they can still be used to keep the observed wavelength centered on the sensor to match other wavelengths.

Finally, a single flat mirror is used to fold the optical path to the science camera sensor. The total optical path length allows the science camera and acquisition camera image planes to be co-planar. This assures that the ORKID footprint did not increase from the original acquisition camera.

4.1.2 Astigmatism Correction

To compensate for other optical paths in the IR path of the AO bench, there is usually an astigmatism term imprinted onto the visible channel beam. To compensate for this, an Astigmatism Corrector Plate (ACP) can be attached to the front of ORKID to apply the correction to the incoming beam. Various ACP plate holders to accommodate different correction scenarios can be attached or removed with a small adjustment in focus to the ORKID stage.

4.1.3 Stray Light Mitigation

Stray light control keeps the image (signal) free of background (noise) that reduce the contrast and resolution of camera output. To accomplish this, baffles are integrated on element mounts (e.g., the triplet and ADCs) and other light paths to the sensors to prevent specular and "single bounce" scatter paths to the sensor. All non-bandpass refractive surfaces are anti-reflection coated to avoid minimize ghost reflections. Analysis shows

any ghosts generated in the system have an extremely low (less than 0.1 percent) contribution to background noise.

4.2 Opto-Mechanical Design

The design of the opto-mechanical components of the ORKID instrument was done in a one month schedule, including the end-of-year holiday, which dictated many of the design choices. The instrument was thus designed to minimize the number of parts to reduce development and fabrication time as well as tolerances stack up. Figure 3 shows an isometric view of the CAD model and the as-built instrument.

The main housing was designed out of a single piece of 6061-T6 aluminum to reduce the number of interfaces and ensure a stiff structure. The cover, also machined from a single piece of aluminum, is mounted on the main housing using captive fasteners. The instrument is mounted on a linear stage (MikroPrecision P/N NE-RS-12) that was used in a previous version of the instrument. An aluminum spacer and shims provide vertical adjustability of the instrument. The ORKID unit is positioned on the spacer via dowel pins to provide a repeatable interface and can be removed independently.

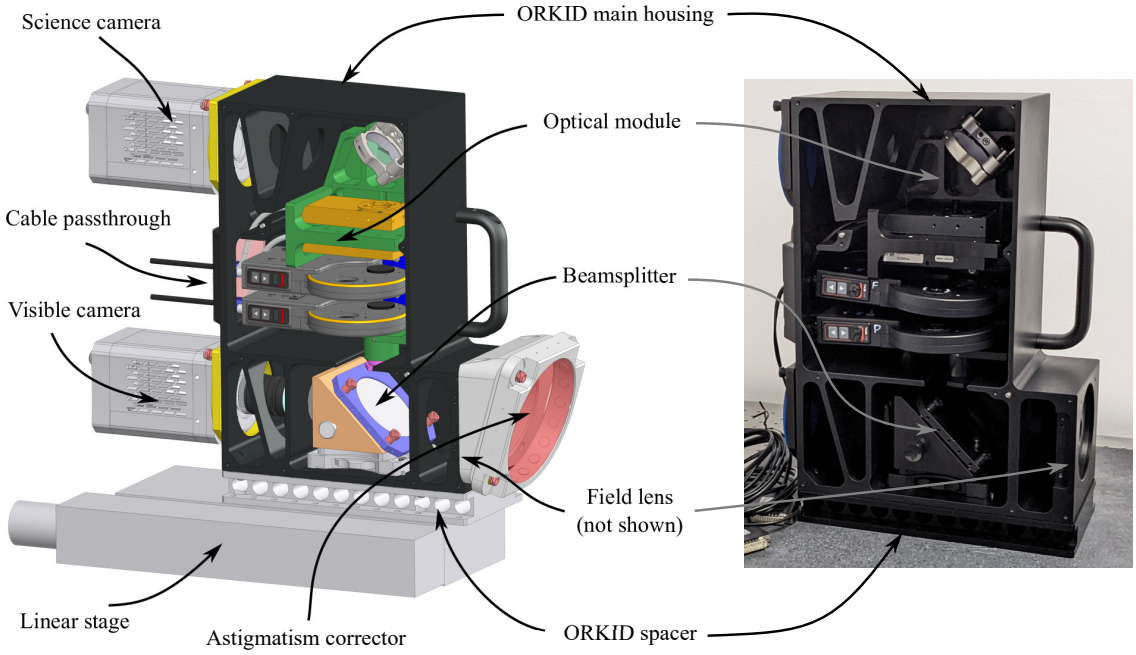

Figure 3. Internal components of the ORKID instrument.

Two Andor cameras (Marana 4B-11) are each mounted on an interface plate that uses three adjustment sleeves to account for the uncertainties of the position of the sensor of the cameras with regard to the mounting features. These sleeves allow adjustment in piston (+/-5mm), pitch and yaw (+/-2deg).

The 100mm field lens (Ross Optical P/N L-PCX391) is mounted directly at the entrance of the main housing and kept in place using an off-the-shelf threaded retaining ring (Thorlabs SM4RR). The curvature of the lens ensures self centering when the retainer ring is installed.

The beamsplitter optic is mounted in a subcell using radial RTV adhesive dots to provide a strain-free mounting. The subcell is mounted on a 45° support using adjustment sleeves that provides three degrees of freedom to the beamsplitter i.e. piston, pitch and yaw. The beamsplitter support is mounted on an off-the-shelf kinematic mount (Newport M-BLK-4) to provide repeatable positioning when the beamsplitter is replaced. Two mounted beamsplitters were provided to test different coatings. Figure 4 shows the beamsplitter mounted in its subcell.

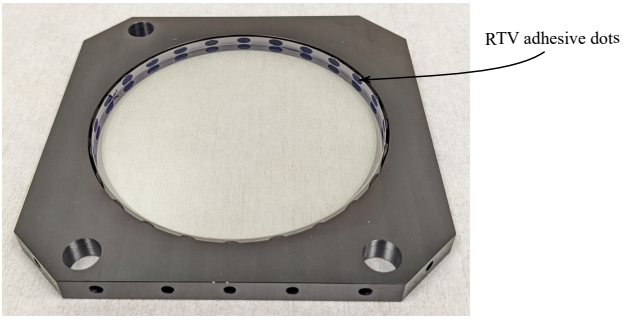

Figure 4. Beamsplitter radially bonded in its mount using RTV adhesive dots.

Following the beamsplitter, the optical module (shown in Figure 5) was designed to mount the motorized components, the custom triplet and the fold mirror. It is precisely located by dowel pins inserted in the main housing.

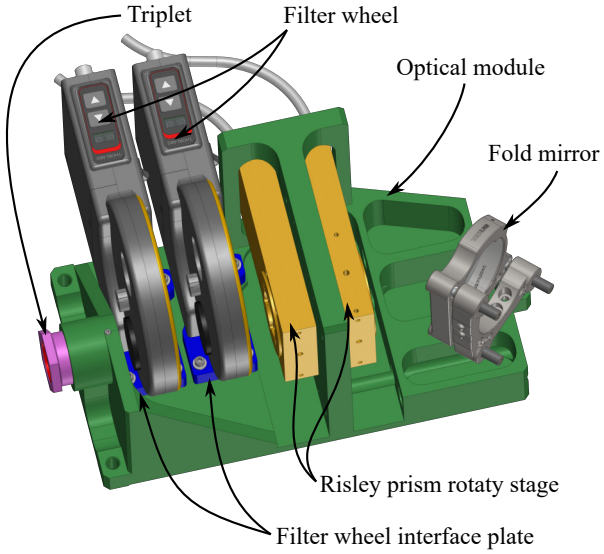

Figure 5. Components included on the optical module.

The triplet is mounted in a subcell that provides adjustability along the optical axis. The clear aperture of the subcell and its retaining ring were tailored to provide stray light reduction. The filter wheels (Thorlabs P/N FW102C) are mounted on interface plates that allow their removal without having to remove the instrument from the AO bench. The interface plates have dowel pins for repeatability and captive fasteners ensure ease of assembly and disassembly. The first filter wheel (called the Pupil Wheel) is perpendicular to the optical path whereas the second filter wheel (called the Filter Wheel) is placed at a 4 degree angle to reduce stray light.

A Pupil Mask shown in Figure 6 needed to be positioned precisely in the Pupil Wheel. Due to the lack of reference features on the off-the-shelf, an alignment tool was designed to use the bearings and the bore of the opposite filter mount to locate the Pupil Mask. Two locating pins on the alignment tool interfaces with a hole and a slot in the Pupil Mask. The alignment tool was printed with a resin printer to ensure a high precision and a good fit. It should be noted that the Pupil Mask is placed on top of an AR-coated 3-mm thick window (shown in green in Figure 6 to maintain the optical path length. A retaining ring is torqued before removing the alignment tool.

Due to the shortage of the chosen baseline rotary stages because of the pandemic situation, the optical module was designed so that two alternative stages (i.e. Phyzik Instrumente U-651 and Newport PR50CC)

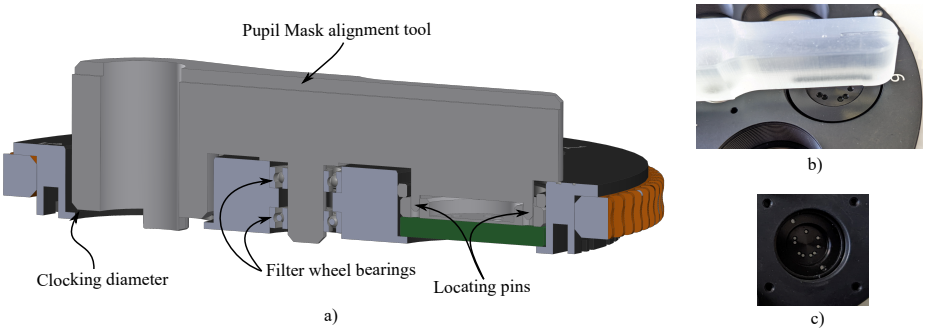

Figure 6. Mask Alignment Jig. a) Cross-section of the CAD model of the alignment tool b)Testing of the alignment tool c)Pupil Mask installed

could integrated on the opto-mechanical module.

Each Risley Prism are mounted in a subcell that is inserted in the a rotary stage. As it can be seen in Figure 7, both subcells are identical and the prisms are held in place with an off-the-shelf retaining ring (Thorlabs SM20RR). The axial placement of the subcells was not critical, so they were placed using a caliper. A retaining ring included with the PR50CC rotary stage acts as a jam nut to the subcell.

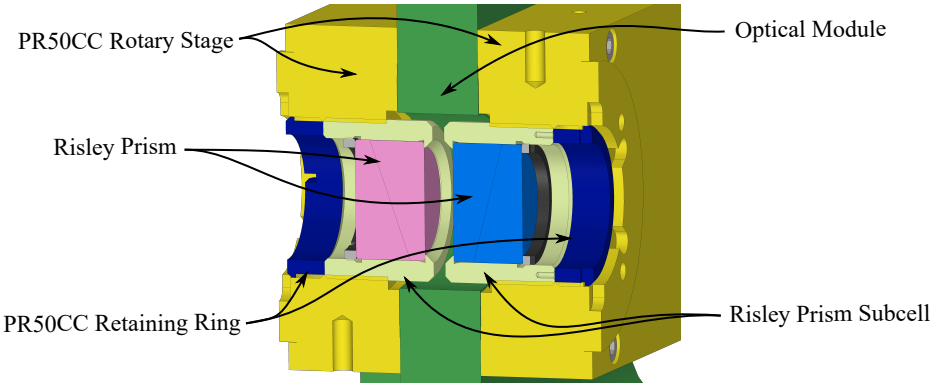

Figure 7. Cross-section of the Risley ADC pair.

The 50mm fold mirror (Thorlabs PF20-03-G01) is mounted in an off-the-shelf kinematic mount (Thorlabs K2) that offers three degrees of freedom i.e. piston, pitch and yaw. in order to reduce the stress on the mirror, it was glued radially in the mount using RTV (Dow Corning 732) and the clamping feature of the mount was not used.

The Astigmatism Corrector Plate was added in front of the field lens. Due to difficulties procuring the optic and the short timeline, a 3D printed support was design to provide the ability to modify it quickly. The printed part integrated machined adjusters and metal threaded inserts to provide adjustability and durability. Similarly to the Beamsplitter, the Astigmatism Corrector Plate is bonded radially in its mount using RTV adhesive dots (as shown in Figure 8).

This modular approach provides a future-proof design to implement improved optical designs with a minimum number of new opto-mechanical components.

Optical tolerances were provided at the beginning of the project to the mechanical team. These requirements were pragmatic and addressed as such by minimizing the number of parts and proper tolerancing of locating features inside and between modules. Not all requirements are met right at assembly but proper adjustment mechanisms were introduced to correct potential dimensional errors. Adjustment mechanisms were be set at their nominal position for initial verification. A simple alignment procedure and related hardware was developed to ensure a quick and proper alignment if nominal positioning is not sufficient.

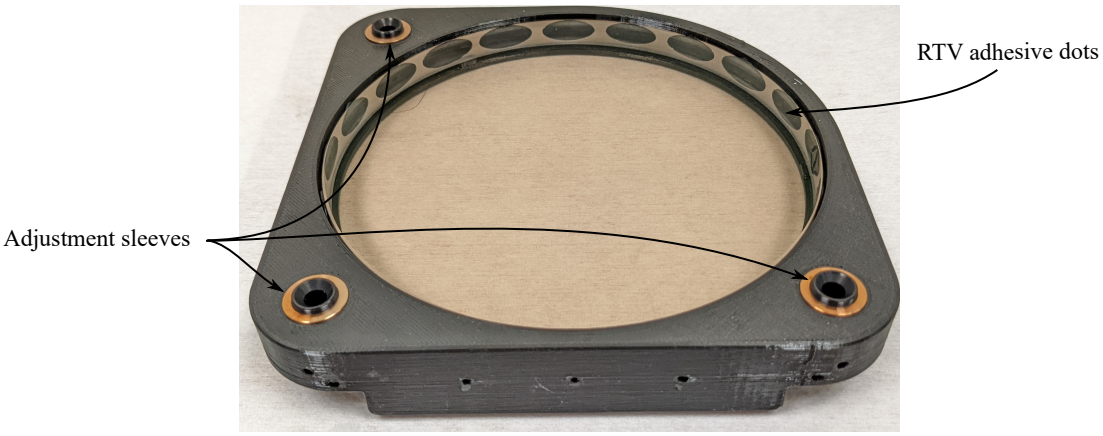

Figure 8. Astigmatism Corrector Plate radially bonded in its 3D printed mount using RTV adhesive dots.

4.3 Filters

Table 1 lists the science filters that have been installed in the ORKID filter wheels.

Table 1. ORKID Bandpass Filters.

WIDEBAND FILTERS	Min	Max
• 27052 R-Band Bessell	554 nm	696 nm
• 27058 i Sloan	698 nm	843 nm
• 27059 z Sloan	830 nm	1000+ nm
NARROWBAND FILTERS	Center	Width
• [OI]	630 nm	10 nm
• H-alpha Continuum Filter	640 nm	6 nm
• 27002 H-alpha	656 nm	5 nm
• 27012 Jovian Methane	889 nm	18 nm
• CT940/20	940 nm	20 nm

4.4 Software Systems Design

The ORKID camera server software is implemented in Python, and combines the interface to the camera with a web server and a keyword server. The web server enables browser-based GUIs, which can be built using readily available tools. The keyword server provides the standard interface that is common to all Keck instruments. The interface to the Andor camera is implemented through the vendor-supplied library, which communicates with the camera via USB. A Python wrapper for this library was built using the CFFI library allowing the software to be written in Python. The main components of the camera servers are:

- Andor camera interface: Interfaces to the vendor provided library
- HTTP web server: Provides web services for the web-based GUI
- Data writer: Provides asynchronous writing of FITS files to disks
- Keck Keywords interface: Retrieves telescope and AO telemetry via keywords and provides the ORKID keyword service

Area of interest (pixel)	Andor Spec max SDR rate (fps)	Measured SDR rate (fps)	Transf SDR rate (MB/sec)	Andor Spec max HDR rate (fps)	Measured HDR rate (fps)	Transf SDR rate (MB/sec)
32x32		738	2		594	1
64x64		594	5		427	4
128x128	750	427	15	378	274	9
256x256	378	274	36	190	159	21
512x512	190	159	84	95	87	46
1024x1024	95	87	181	30	45	95
2048x2048	48	45	211*	24	23	194

Table 2. Maximum frame rate for different areas of interest. *Lower rate due to dropped frames.

- Control GUI: Web-based GUI to control and monitor the camera, as well as to display the images.

The selected camera is the Andor Marana by Oxford Instruments. Table 1 shows the frame rates for different areas of interest. The Andor Marana specification gives the maximum frame rates. The actual frame rates are measured using the current implementation of the camera server for SDR (12 bit) and HDR (16 bit) read out modes.

The frames from the camera are saved to disk in FITS format at the maximum transfer rate of 211 MB/sec. This requires the use of fast disk storage systems. Fortunately, commercial available SSDs (Solid-State Disks) such as the Samsung PM893 7TB, can achieve 530 MB/sec write speed. To decouple the synchronous readout of the camera frames from the fluctuation of the data I/O process a FIFO data queue is used.

5. PERFORMANCE ANALYSIS

The optical performance of ORKID meets the science goals of having a FWHM ¡2 pixels at 650 nm. This is achieved by diffraction-limited design with an RMS wavefront error below 50 nm. This is shown in Figures 9 and 10.

APPENDIX A. MATERIALS AND METHODS

This section will provide an overview of how the database was compiled and used to produce figures, etc.

ACKNOWLEDGMENTS

This unnumbered section is used to identify those who have aided the authors in understanding or accomplishing the work presented and to acknowledge sources of funding.

The W. M. Keck Observatory is operated as a scientific partnership among the California Institute of Technology, the University of California, and the National Aeronautics and Space Administration. The Observatory was made possible by the generous financial support of the W. M. Keck Foundation.

The authors wish to recognize and acknowledge the very significant cultural role and reverence that the summit of Maunakea has always had within the indigenous Hawaiian community. We are most fortunate to have the opportunity to conduct observations from this mountain.

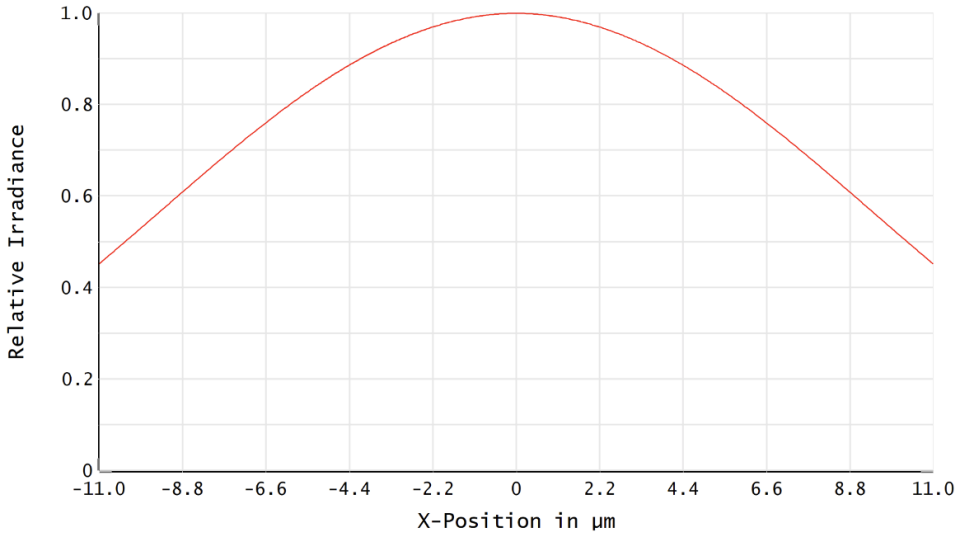

Figure 9. The ORKID FWHM is ¡2 pixels (22 µm).

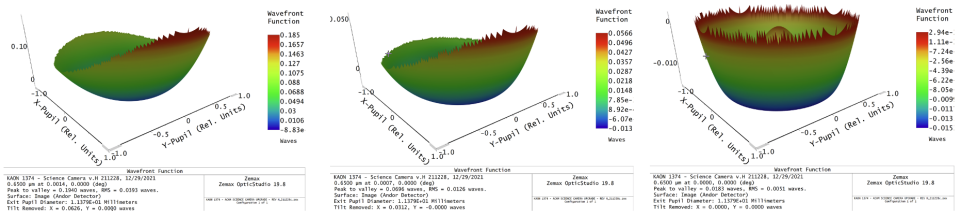

Figure 10. The wavefront error is ¡50 nm RMS across the field.

Additional references:

First Light Adaptive Optics Images from the Keck II Telescope: A New Era of High Angular Resolution Imagery. P. Wizinowich, D.S. Acton, C. Shelton, P. Stomski, J. Gathright, K. Ho, W. Lupton, K. Tsubota, O. Lai, C. Max, J. Brase, J. An, K. Avicola, S. Olivier, D. Gavel, B. Macintosh, A. Ghez J. Larkin. Publications of the Astronomical Society of the Pacific, Vol. 112, 315-319 (2000).

The W. M. Keck Observatory Laser Guide Star Adaptive Optics System: Overview. P. Wizinowich, D. Le Mignant, A. Bouchez, R. Campbell, J. Chin, A. Contos, M van Dam, S. Hartman, E. Johansson, R. Lafon, H. Lewis, P. Stomski, D. Summers, C. Brown, P. Danforth, C. Max, D. Pennington. Publications of the Astronomical Society of the Pacific, 118:297-309 (2006).

Adaptive optics with an infrared pyramid wavefront sensor at Keck. Charlotte Z. Bond, Sylvain Cetre, Scott Lilley, Peter Wizinowich, Dimitri Mawet, Mark Chun, Edward Wetherell, Shane Jacobson, Charles Lockhart, Eric Warmbier, Sam Ragland, Carlos Alvarez, Olivier Guyon, Sean Goebel, Jacques-Robert Delorme, Nemanja Jovanovic, Donald N. Hall, James K. Wallace, Mojtaba Taheri, Cedric Plantet, and Vincent Chambouleyron. J. Astron. Telesc. Instrum. Syst. 6, 039003 (2020).

REFERENCES

[1] Smith, B. A., Soderblom, L. A., Beebe, R., Bliss, D., Boyce, J. M., Brahic, A., Briggs, G. A., Brown, R. H., Collins, S. A., Cook, A. F., Croft, S. K., Cuzzi, J. N., Danielson, G. E., Davies, M. E., Dowling, T. E., Godfrey, D., Hansen, C. J., Harris, C., Hunt, G. E., Ingersoll, A. P., Johnson, T. V., Krauss, R. J., Masursky, H., Morrison, D., Owen, T., Plescia, J. B., Pollack, J. B., Porco, C. C., Rages, K., Sagan, C., Shoemaker, E. M., Sromovsky, L. A., Stoker, C., Strom, R. G., Suomi, V. E., Synnott, S. P., Terrile, R. J., Thomas, P., Thompson, W. R., and Veverka, J., "Voyager 2 in the Uranian System: Imaging Science Results," *Science* **233**, 43–64 (July 1986).

[2] Smith, B. A., Soderblom, L. A., Banfield, D., Barnet, C., Basilevksy, A. T., Beebe, R. F., Bollinger, K., Boyce, J. M., Brahic, A., Briggs, G. A., Brown, R. H., Chyba, C., Collins, S. A., Colvin, T., Cook, A. F., Crisp, D., Croft, S. K., Cruikshank, D., Cuzzi, J. N., Danielson, G. E., Davies, M. E., de Jong, E., Dones, L., Godfrey, D., Goguen, J., Grenier, I., Haemmerle, V. R., Hammel, H., Hansen, C. J., Helfenstein, C. P., Howell, C., Hunt, G. E., Ingersoll, A. P., Johnson, T. V., Kargel, J., Kirk, R., Kuehn, D. I., Limaye, S., Masursky, H., McEwen, A., Morrison, D., Owen, T., Owen, W., Pollack, J. B., Porco, C. C., Rages, K., Rogers, P., Rudy, D., Sagan, C., Schwartz, J., Shoemaker, E. M., Showalter, M., Sicardy, B., Simonelli, D., Spencer, J., Sromovsky, L. A., Stoker, C., Strom, R. G., Suomi, V. E., Synott, S. P., Terrile, R. J., Thomas, P., Thompson, W. R., Verbiscer, A., and Veverka, J., "Voyager 2 at Neptune: Imaging Science Results," *Science* **246**, 1422–1449 (Dec. 1989).

[3] de Pater, I., Sromovsky, L. A., Fry, P. M., Hammel, H. B., Baranec, C., and Sayanagi, K. M., "Record-breaking storm activity on Uranus in 2014," **252**, 121–128 (May 2015).

[4] Molter, E., de Pater, I., Luszcz-Cook, S., Hueso, R., Tollefson, J., Alvarez, C., Sánchez-Lavega, A., Wong, M. H., Hsu, A. I., Sromovsky, L. A., Fry, P. M., Delcroix, M., Campbell, R., de Kleer, K., Gates, E., Lynam, P. D., Ammons, S. M., Coy, B. P., Duchene, G., Gonzales, E. J., Hirsch, L., Magnier, E. A., Ragland, S., Rich, R. M., and Wang, F., "Analysis of Neptune's 2017 bright equatorial storm," **321**, 324–345 (Mar. 2019).

[5] Sallum, S., Follette, K. B., Eisner, J. A., Close, L. M., Hinz, P., Kratter, K., Males, J., Skemer, A., Macintosh, B., Tuthill, P., Bailey, V., Defrère, D., Morzinski, K., Rodigas, T., Spalding, E., Vaz, A., and Weinberger, A. J., "Accreting protoplanets in the LkCa 15 transition disk," **527**, 342–344 (Nov. 2015).

[6] Mendigutía, I., Oudmaijer, R. D., Schneider, P. C., Huélamo, N., Baines, D., Brittain, S. D., and Aberasturi, M., "Spectro-astrometry of the pre-transitional star LkCa 15 does not reveal an accreting planet but extended Hα emission," **618**, L9 (Oct. 2018).

[7] Currie, T., Marois, C., Cieza, L., Mulders, G. D., Lawson, K., Caceres, C., Rodriguez-Ruiz, D., Wisniewski, J., Guyon, O., Brandt, T. D., Kasdin, N. J., Groff, T. D., Lozi, J., Chilcote, J., Hodapp, K., Jovanovic, N., Martinache, F., Skaf, N., Lyra, W., Tamura, M., Asensio-Torres, R., Dong, R., Grady, C., Gerard, B., Fukagawa, M., Hand, D., Hayashi, M., Henning, T., Kudo, T., Kuzuhara, M., Kwon, J., McElwain, M. W., and Uyama, T., "No Clear, Direct Evidence for Multiple Protoplanets Orbiting LkCa 15: LkCa 15 bcd are Likely Inner Disk Signals," **877**, L3 (May 2019).

[8] Haffert, S. Y., Bohn, A. J., de Boer, J., Snellen, I. A. G., Brinchmann, J., Girard, J. H., Keller, C. U., and Bacon, R., "Two accreting protoplanets around the young star PDS 70," *Nature Astronomy* **3**, 749–754 (June 2019).

[9] Zhou, Y., Bowler, B. P., Wagner, K. R., Schneider, G., Apai, D., Kraus, A. L., Close, L. M., Herczeg, G. J., and Fang, M., "Hubble Space Telescope UV and Hα Measurements of the Accretion Excess Emission from the Young Giant Planet PDS 70 b," **161**, 244 (May 2021).

[10] Eriksson, S. C., Asensio Torres, R., Janson, M., Aoyama, Y., Marleau, G.-D., Bonnefoy, M., and Petrus, S., "Strong Hα emission and signs of accretion in a circumbinary planetary mass companion from MUSE," **638**, L6 (June 2020).

[11] Cugno, G., Quanz, S. P., Hunziker, S., Stolker, T., Schmid, H. M., Avenhaus, H., Baudoz, P., Bohn, A. J., Bonnefoy, M., Buenzli, E., Chauvin, G., Cheetham, A., Desidera, S., Dominik, C., Feautrier, P., Feldt, M., Ginski, C., Girard, J. H., Gratton, R., Hagelberg, J., Hugot, E., Janson, M., Lagrange, A. M., Langlois, M., Magnard, Y., Maire, A. L., Menard, F., Meyer, M., Milli, J., Mordasini, C., Pinte, C., Pragt, J., Roelfsema, R., Rigal, F., Szulágyi, J., van Boekel, R., van der Plas, G., Vigan, A., Wahhaj, Z., and Zurlo, A., "A search for accreting young companions embedded in circumstellar disks. High-contrast Hα imaging with VLT/SPHERE," **622**, A156 (Feb. 2019).

[12] Zurlo, A., Cugno, G., Montesinos, M., Perez, S., Canovas, H., Casassus, S., Christiaens, V., Cieza, L., and Huelamo, N., "The widest Hα survey of accreting protoplanets around nearby transition disks," **633**, A119 (Jan. 2020).

[13] Bond, C. Z., Cetre, S., Lilley, S., Wizinowich, P., Mawet, D., Chun, M., Wetherell, E., Jacobson, S., Lockhart, C., Warmbier, E., Ragland, S., Alvarez, C., Guyon, O., Goebel, S., Delorme, J.-R., Jovanovic, N., Hall, D. N., Wallace, J. K., Taheri, M., Plantet, C., and Chambouleyron, V., "Adaptive optics with

an infrared pyramid wavefront sensor at Keck," *Journal of Astronomical Telescopes, Instruments, and Systems* **6**, 039003 (July 2020).

[14] Rodriguez, C., Taylor, G. B., Zavala, R. T., Peck, A. B., Pollack, L. K., and Romani, R. W., "A Compact Supermassive Binary Black Hole System," **646**, 49–60 (July 2006).

[15] Satyapal, S., Secrest, N. J., Ricci, C., Ellison, S. L., Rothberg, B., Blecha, L., Constantin, A., Gliozzi, M., McNulty, P., and Ferguson, J., "Buried AGNs in Advanced Mergers: Mid-infrared Color Selection as a Dual AGN Candidate Finder," **848**, 126 (Oct. 2017).

[16] Pfeifle, R. W., Satyapal, S., Secrest, N. J., Gliozzi, M., Ricci, C., Ellison, S. L., Rothberg, B., Cann, J., Blecha, L., Williams, J. K., and Constantin, A., "Buried Black Hole Growth in IR-selected Mergers: New Results from Chandra," **875**, 117 (Apr. 2019).

[17] Koss, M., Mushotzky, R., Veilleux, S., Winter, L. M., Baumgartner, W., Tueller, J., Gehrels, N., and Valencic, L., "Host Galaxy Properties of the Swift Bat Ultra Hard X-Ray Selected Active Galactic Nucleus," **739**, 57 (Oct. 2011).

[18] Koss, M. J., Blecha, L., Bernhard, P., Hung, C.-L., Lu, J. R., Trakhtenbrot, B., Treister, E., Weigel, A., Sartori, L. F., Mushotzky, R., Schawinski, K., Ricci, C., Veilleux, S., and Sanders, D. B., "A population of luminous accreting black holes with hidden mergers," **563**, 214–216 (Nov. 2018).